Clinical and Translational Report

Cell Metabolism

Postprandial Oxidative Metabolism of Human Brown Fat Indicates Thermogenesis

Graphical Abstract

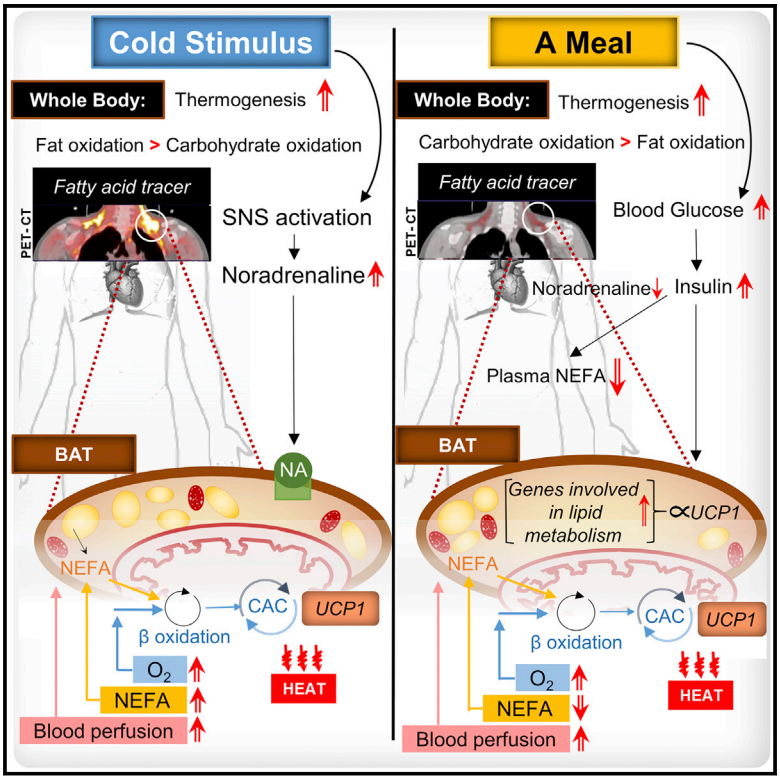

Highlights

- A carbohydrate-dominant meal triggers human brown fat thermogenesis
- After a meal, the genes involved in fatty acid metabolism are highly expressed in BAT
- BAT uptake of circulatory fatty acids after meal consumption is minimal
- Postprandial thermogenesis in BAT is linked to circulatory fatty acid uptake

Authors

Mueez U Din, Teemu Saari, Juho Raiko, ..., Olof Solin, Pirjo Nuutila, Kirsi A. Virtanen

Correspondence

kirsi.virtanen@utu.fi

In Brief

Using PET/CT imaging, U Din et al. show that eating a carbohydrate-rich meal triggers human brown adipose tissue (hBAT) thermogenesis to the same extent as cold stress, though the substrates used are different. Glucose and LPL-derived fatty acids are preferentially taken up by hBAT in the postprandial state.

U Din et al., 2018, Cell Metabolism *28*, 207–216
August 7, 2018
https://doi.org/10.1016/j.cmet.2018.05.020

CellPress

Cell Metabolism
Clinical and Translational Report

Postprandial Oxidative Metabolism of Human Brown Fat Indicates Thermogenesis

Mueez U Din,[1,2,11] Teemu Saari,[1,2,11] Juho Raiko,[1,2] Nobu Kudomi,[3] Stefanie F. Maurer,[4] Minna Lahesmaa,[1,2] Tobias Fromme,[4] Ez-Zoubir Amri,[5] Martin Klingenspor,[4,6] Olof Solin,[1,2,7,8] Pirjo Nuutila,[1,2,9] and Kirsi A. Virtanen[1,2,10,12,*]
[1]Turku PET Centre, Turku University Hospital, Kiinamyllynkatu 4-8, 20520 Turku, Finland
[2]Turku PET Centre, University of Turku, Kiinamyllynkatu 4-8, 20520 Turku, Finland
[3]Department of Medical Physics, Faculty of Medicine, Kagawa University, Takamatsu, Kagawa, Japan
[4]Chair of Molecular Nutritional Medicine, Else Kröner-Fresenius Center, Technical University of Munich, 85354 Freising, Germany
[5]University Côte d'Azur, CNRS, Inserm, iBV, Nice, France
[6]ZIEL – Institute for Food and Health, Technical University of Munich, 85354 Freising, Germany
[7]Department of Chemistry, University of Turku, Turku, Finland
[8]Accelerator Laboratory, Åbo Akademi University, Turku, Finland
[9]Department of Endocrinology, Turku University Hospital, Turku, Finland
[10]Institute of Public Health and Clinical Nutrition, University of Eastern Finland (UEF), Kuopio, Finland
[11]These authors contributed equally
[12]Lead Contact
*Correspondence: kirsi.virtanen@utu.fi
https://doi.org/10.1016/j.cmet.2018.05.020

SUMMARY

Human studies suggest that a meal elevates glucose uptake in brown adipose tissue (BAT). However, in postprandial state the thermogenic activity and the metabolism of non-esterified fatty acids (NEFAs) in BAT remain unclear. Using indirect calorimetry combined with positron emission tomography and computed tomography (PET/CT), we showed that whole-body and BAT thermogenesis (oxygen consumption) increases after the ingestion of a mixed carbohydrate-rich meal, to the same extent as in cold stress. Postprandial NEFA uptake into BAT is minimal, possibly due to elevated plasma insulin inhibiting lipolysis. However, the variation in postprandial NEFA uptake is linked to BAT thermogenesis. We identified several genes participating in lipid metabolism to be expressed at higher levels in BAT compared with white fat in postprandial state, and to be positively correlated with BAT *UCP1* expression. These findings suggest that substrates preferred by BAT in postprandial state are glucose or LPL-released NEFAs due to insulin stimulation.

INTRODUCTION

Brown adipose tissue (BAT) is considered a vital organ for a contributory role in non-shivering heat production both in rodents and humans (Himms-Hagen, 1984). BAT has been observed to be active during cold stress, in response to sympathetic nervous system activation, based on high metabolic activity visualized on positron emission tomography (PET) imaging using various radiotracers (Orava et al., 2013; Ouellet et al., 2012; Virtanen et al., 2009). Human whole-body thermogenesis has been linked with BAT activity during cold stress (Chen et al., 2013; van Marken Lichtenbelt et al., 2009; Yoneshiro et al., 2011), thus advocating the role of BAT as a thermoregulatory organ.

BAT produces heat owing to the presence of uncoupling protein 1 *(UCP1)* protein within mitochondria (Nedergaard et al., 2001). It has been postulated that the presence of active BAT may also act as an energy sink in order to maintain long-term energy balance (Rothwell and Stock, 1979), and indeed the loss of thermogenic BAT function caused increased diet-induced obesity in mice (Feldmann et al., 2009; Kontani et al., 2005), although this was not found in other studies (Liu et al., 2003; Olsen et al., 2017). Pertaining to acute meal-induced thermogenesis, several rodent studies have shown that the consumption of a single meal triggers BAT activation (Allard and Leblanc, 1988; Glick and Raum, 1986; Glick et al., 1981, 1983, 1984, 1985; Lupien et al., 1985).

In humans, the role of BAT in postprandial metabolism is unclear, and additionally the notion of whether BAT functions as an organ for energy balance remains controversial (Kozak, 2010; Peterson et al., 2017). The study by Vosselman et al. (2013) has demonstrated that a high-caloric carbohydrate-rich meal stimulates BAT glucose uptake. However, due to static PET measurement, the volume of glucose utilization could not be measured; accordingly, quantitative contribution of BAT in comparison with additional tissues (muscles and white adipose tissue) could not be estimated. Moreover, it could not be established whether glucose taken up postprandially in BAT further undergoes mitochondrial oxidation (i.e., *UCP1*-mediated heat production). Since BAT is considered to be relying majorly on both endogenous and exogenous non-esterified fatty acids (NEFAs) for substrate oxidation (Ma and Foster, 1986; Muzik et al., 2013; U Din et al., 2016), evaluation of BAT fatty acid metabolism following meal consumption remains crucial as well.

In order to elucidate the postprandial activation of BAT, and contributory role of BAT in meal-induced thermogenesis, we studied 16 healthy human adults subsequent to carbohydrate-dominant mixed meal ingestion with dynamic PET-computed

Table 1. Characteristics of Study Subjects

	Control Group	Experimental Group	p Value[a]
No.	9	16	–
Sex (female/male)	4/5	12/4	–
Age (years)	36.3 ± 9.3	35.4 ± 11.3	0.83
Weight (kg)	78.7 ± 14.0	76.9 ± 14.6	0.77
BMI (kg/m^2)	26.1 ± 3.1	27.3 ± 3.9	0.44
Waist (cm)	89.9 ± 9.2	92.9 ± 16.0	0.62
HbA1C (%)	5.1 ± 0.2	5.3 ± 0.4	0.28
Insulin sensitivity (M value) (μmol/kg/min)	38.0 ± 21	45.0 ± 22.8	0.47
Whole-body fat percentage (%)	28.1 ± 10.3	34.3 ± 8.0	0.10
BAT radiodensity (cold, HU)	−85.5 ± 6.9	−86.4 ± 7.8	0.76
BAT mass (g)	113 ± 68	113 ± 67	1.00

[a]Unpaired Student's t test

tomography (CT) scanning using [^{15}O]O_2, [^{15}O]H_2O, and [^{18}F]FTHA radiotracers to determine the rates of oxygen consumption, blood flow, and circulatory NEFA uptake, respectively. The advantage with dynamic PET acquisitions is the possibility to non-invasively quantify the rate as well as the volume of substrate/radiotracer consumption. Postprandial CT radiodensity of BAT was measured in order to have an insight into BAT intracellular lipid metabolism (Ouellet et al., 2012; U Din et al., 2017). In addition, whole-body postprandial energy expenditure was determined using an indirect respiratory calorimeter. The measurements were repeated after an overnight fasting during a mild cold stress, which provided paired positive control comparison. Additionally, the identical experiments were performed on a control group (n = 9; Table 1) after an overnight fasting at room temperature, which provided negative control comparison (Figure 1).

RESULTS AND DISCUSSION

Meal Increases Oxygen Consumption and Blood Flow of BAT

Measurement of oxygen consumption provides direct evidence for the underlying mitochondrial respiratory chain reactions irrespective of the choice of substrate utilization. The benefit of using [^{15}O]O_2 PET radiotracer, in particular, is the bulk availability to all tissues, which is not influenced by "stealing phenomena" by muscles, as might be the case with [^{18}F]FDG, reported earlier (Vosselman et al., 2013; Vrieze et al., 2012). Postprandial oxygen consumption of supraclavicular BAT was similar to that during the cold stimulation (p = 0.99), though the oxygen consumption of BAT in both states (postprandial and cold) was significantly higher than the room temperature measurements (postprandial, p = 0.01; cold, p = 0.01; Figure 2A). Likewise, BAT blood flow was elevated in the postprandial and cold-stimulated states (postprandial versus cold, p = 0.39) and significantly higher than the negative control conditions (postprandial, p = 0.01; cold, p = 0.004; Figure 2B). These findings support that BAT is hypermetabolic after taking a mixed meal.

The oxygen consumption of posterior subcutaneous white adipose tissue (WAT) (neck level) in postprandial state was significantly higher than in the negative control conditions (p = 0.01), but no difference was observed between cold versus negative control (p = 0.47) and cold versus postprandial conditions (p = 0.60). The blood flow in posterior subcutaneous WAT (neck level) in postprandial state was significantly higher than during cold (p = 0.02), while no difference was observed in postprandial versus fasting state (negative control, p = 0.16; Figure 2B). While posterior subcutaneous WAT may be prone to measurement artifact due to the compression of supine body, we also analyzed oxygen consumption and blood flow of the lateral subcutaneous WAT (arm level). However, this was possible only in a part of the study subjects (Figure S1). These data showed a lower magnitude in oxygen consumption and blood flow compared with posterior subcutaneous WAT, while no significant differences were observed within cold, control (fasting), and postprandial states.

Cervico-thoracic muscles contribute to cold-induced non-shivering thermogenesis in humans (U Din et al., 2016). Therefore, as a comparative measure, we analyzed several muscles located in the field of view (FOV) of the PET-CT scanner. In postprandial state, the blood flow toward the cervico-thoracic muscles was not higher compared with negative control measurements. The increased blood flow toward levator scapular and pectoralis major muscle, the centrally located cervico-thoracic muscles, could only be seen during the cold stress (both $p < 0.05$), while we did not find cold-induced elevation in blood flow of splenius cervicis, trapezius, and deltoid muscles (Figure 2B). Similarly, the oxygen consumption in cervico-thoracic muscles during cold stimulation was found to be significantly elevated only in levator scapulae and pectoralis major muscle (both $p < 0.05$), while no statistical difference was observed in splenius cervicis, trapezius, or deltoid muscles. In postprandial state, oxygen consumption of the muscles was not different from the negative control measurements (with the only exception of pectoralis major muscle) (Figure 2A). The relationship between oxygen consumption and blood flow is depicted in Figures S2 and S3. Postprandial oxygen consumption and blood flow correlated positively in BAT, WAT, and all analyzed skeletal muscles.

Meal Suppresses Circulatory NEFA Uptake in BAT, WAT, and Muscles

Net influx rate of [^{18}F]FTHA (K_i) represents the amount of accumulated tracer in the tissue compared with the amount of tracer available in plasma. Postprandial net influx rate of [^{18}F]FTHA (K_i) was significantly higher in BAT, WAT, and all analyzed cervico-thoracic muscles (except pectoralis major) compared with negative control (fasting state), as well as cold-stimulated measurements ($p < 0.05$; Figure 2C). In pectoralis major muscle, there was no significant difference between cold versus postprandial measurement (p = 0.59; Figure 2C).

Since [^{18}F]FTHA is a trapping palmitate analogue, tissue-specific NEFA uptake is a product of K_i and arterial plasma NEFA concentration during the scanning (blood sampling time point 2, as shown in Figure 1). The plasma NEFA concentrations decreased significantly after the meal, and as a result, tissue-specific NEFA uptake rates (in all tissues within our PET-CT

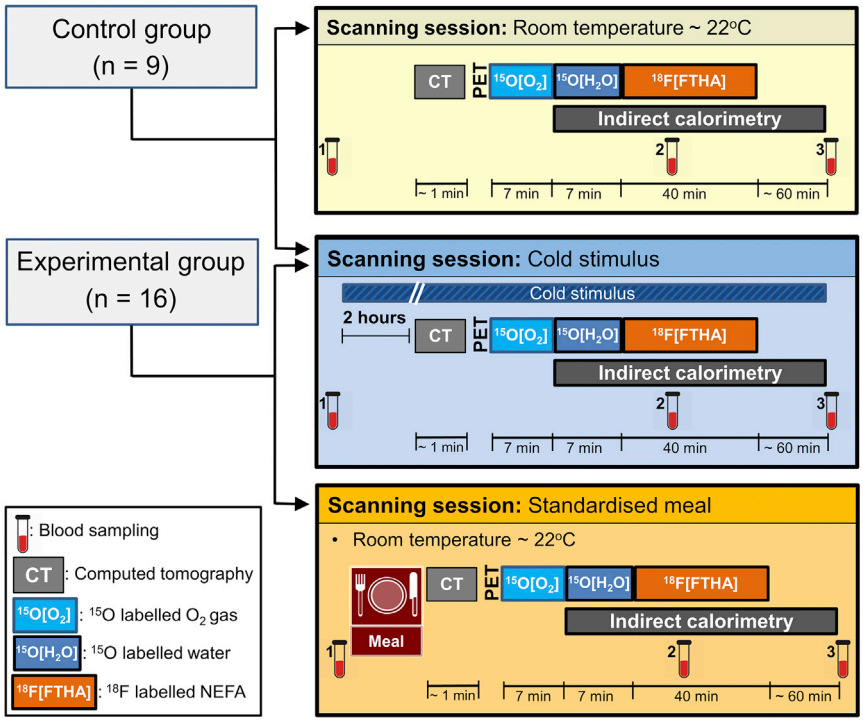

Figure 1. Diagrammatic Representation of Study Design

Two separate groups of human subjects participated in the study. The subjects in experimental group were scanned at two different sessions. In one session, the subjects were given cold stimulus with overnight fasting, while in another scanning session, subjects were scanned after the ingestion of a standardized meal at room temperature. The subjects in the control group were scanned after an overnight fasting by giving cold stimulus (positive control condition) and without cold stimulus at room temperature (negative control condition). All scanning sessions had similar scanning protocol in which subjects were scanned with attenuation correction CT and afterward with PET using three radiotracers: $[^{15}O]O_2$, $[^{15}O]H_2O$, and $[^{18}F]$FTHA. Indirect respiratory calorimetry was also performed, which continued after scanning as well; moreover, blood samples were drawn at three scheduled time points.

FOV) were significantly lower than negative control and cold-stimulated state ($p < 0.05$; Figures 2D–2F). Cold stimulus induced a higher NEFA uptake in BAT, trapezius, levator scapulae, splenius cervicis, and pectoralis major muscles compared with room temperature measurement ($p < 0.05$; Figure 2D). However, no cold-induced effect on NEFA uptake was observed in WAT and deltoid muscle (Figure 2D). Postprandial net influx rate of $[^{18}F]$FTHA (K_i) in BAT was inversely related to postprandial plasma NEFA concentrations (time point 2: mid-scan) (*rho* = −0.54, $p = 0.03$; Figure 2G). It is possible that the low levels of plasma NEFAs cause BAT to take up all available NEFAs, thus increasing the net influx rate (K_i). Additionally, postprandial BAT NEFA uptake was in direct relationship with BAT oxygen consumption ($r = 0.795$, $p = 0.002$) and BAT blood flow ($r = 0.86$, $p < 0.001$; Figure 2H). Although NEFA uptake (K_i multiplied with plasma NEFAs) is suppressed in BAT, these findings still suggest that postprandial BAT thermogenesis is linked with BAT circulatory NEFA uptake.

The study by Vosselman et al. (2013) has shown that glucose uptake in BAT after a high-calorie carbohydrate-dense meal was comparable to that after a cold stimulus, and additionally they found a direct relationship between plasma insulin concentrations and BAT glucose uptake marker (SUVs). The latter possibly suggests that an increase in insulin receptor signaling triggers increased glucose uptake of BAT, likely serving as a primary substrate of postprandial BAT thermogenesis. We have previously shown that BAT is an insulin-sensitive tissue (Orava et al., 2011), and insulin stimulation results in increased glucose uptake in BAT. The study by Vrieze et al. (2012) has shown decreased BAT $[^{18}F]$FDG uptake in the postprandial state compared with fasting; however, the study used the cold stimulation in the postprandial state, making the direct comparison to our study challenging.

Meal Increases Whole-Body Thermogenesis

Whole-body energy expenditure (EE) was higher after cold stimulus ($p = 0.02$) compared with negative control, and it was elevated to the same level as in the postprandial state (cold versus postprandial, $p = 0.27$; Figure 3A). Postprandial whole-body EE per lean body mass (fat-free mass, FFM) was significantly higher than the negative control ($p < 0.001$; Figure 3B). The phenomenon of meal-induced thermogenesis has been reported previously (Tentolouris et al., 2011; Vosselman et al., 2013; Westerterp et al., 1999), and this post-meal increase in EE is likely due to the increased ATP production required for the metabolic processes of intestinal absorption, nutrient storage, and conversions (Tappy, 1996).

There was a significant difference in the preference of substrate oxidation among postprandial, negative control, and cold-stimulated states, as reflected in different respiratory quotients (RQs) (postprandial versus negative control and postprandial versus cold, $p < 0.001$; Figure 3C). RQs tended to be lower in cold compared with negative control ($p = 0.066$). The whole-body carbohydrate oxidation was dominant in postprandial state when compared with negative control and cold conditions ($p < 0.001$; Figures 3D and 3E). Instead, in cold, the whole-body fat oxidation dominated and was significantly higher when compared with negative control and postprandial state ($p < 0.0001$; Figures 3D and 3E). Whole-body fat oxidation was suppressed in postprandial state compared with negative control and cold conditions ($p < 0.001$; Figures 3D and 3E). The dominance of whole-body carbohydrate oxidation also supports that BAT is likely oxidizing glucose in the postprandial state.

Once the subjects were categorized into high BAT and low BAT based on cold-stimulated BAT NEFA uptake (high BAT, NEFA uptake rate ≥ 0.7 μmol/100 g/min), significantly higher postprandial whole-body EE (per FFM) and postprandial whole-body carbohydrate oxidation (per FFM) were observed in high-BAT subjects compared with low-BAT subjects

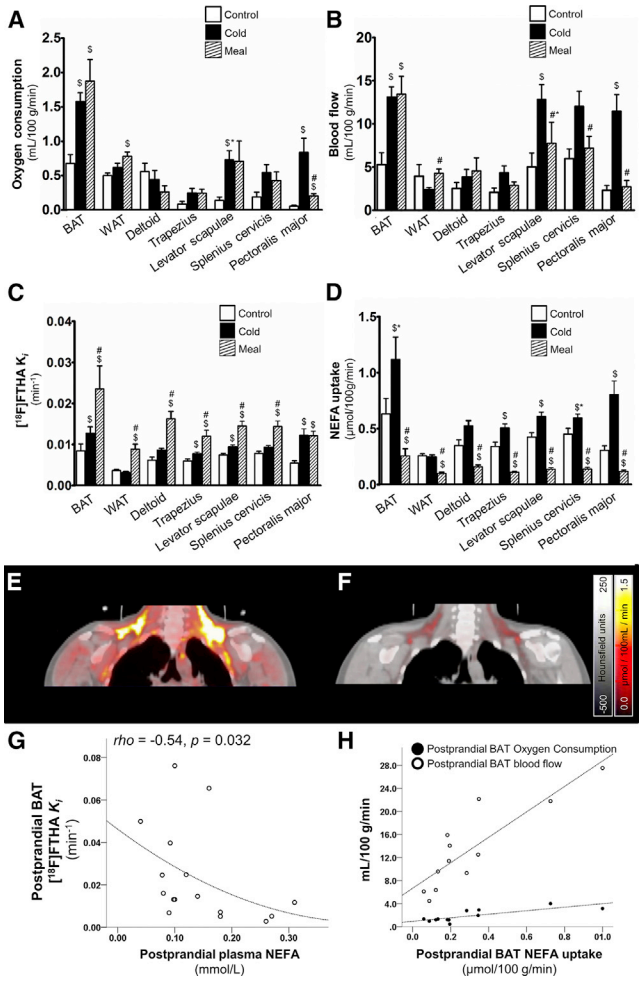

Figure 2. Oxygen Consumption, Blood Flow, and NEFA Uptake

(A) Oxygen consumption, measured with [^{15}O]O_2 PET in supraclavicular BAT, posterior subcutaneous WAT (neck level), and cervico-thoracic muscles, at control conditions, during mild cold stress, and after a meal intake.

(B) Blood flow, measured by [^{15}O]H_2O PET, in supraclavicular BAT, posterior subcutaneous WAT (neck level), and cervico-thoracic muscles, at control conditions, during mild cold stress, and after a meal intake.

(C) [^{18}F]FTHA net influx rates (K_i) of BAT, WAT and cervico-thoracic muscles acquired from graphical analysis of PET data.

(D) NEFA uptake in BAT, WAT, and cervico-thoracic muscles.

(E and F) Representative coronal image of the cervico-thoracic region fused PET-CT image scanned during cold stress (E) and after taking a meal (F).

(G) Postprandial BAT K_i was inversely related to plasma NEFA concentrations.

(H) Postprandial BAT NEFA uptake was found to be significantly correlating with postprandial BAT oxygen consumption (r = 0.82, p = 0.001) and postprandial BAT blood flow (r = 0.90, p < 0.0001).

Results are presented as means ± SEM. $, significantly different from negative control (p < 0.05); #, significant difference between cold and meal measurements (p < 0.05); *, Wilcoxon rank-sum test. See also Figures S1–S3.

(p = 0.02 and p = 0.004, respectively; Figure 3F). No significant difference was observed in postprandial whole-body fat oxidation in these subjects (p = 0.13; Figure 3F). This finding is in line with a previous report (Hibi et al., 2016) in which the BAT-positive study subjects had higher postprandial metabolic rate (average +5 kcal/day/kg FFM). However, this finding in our study may be influenced by the fact that high-BAT subjects had better whole-body insulin sensitivity (M value) and M value correlated with whole-body carbohydrate oxidation (per FFM) (r = 0.67, p = 0.01).

Hormones, Metabolites, Skin Temperature, and BAT Composition Measurements

Mixed meal stimulated insulin secretion due to an increase in plasma glucose level (p < 0.0001), whereas plasma insulin concentration was lower during cold and fasting states and further dropped significantly compared with the baseline in both cold stimulus and negative control scanning sessions (p < 0.05; Figure 4A) without any change in plasma glucose (Figure 4B). Plasma NEFA level dropped significantly after meal consumption, while it rose significantly in response to cold stimulus; no change was noticed during the negative control scanning session (Figure 4C). Cold increased plasma noradrenaline almost 2-fold (p < 0.0001; Figure 4D), but not adrenaline levels (Figure 4E). In contrast, plasma noradrenaline decreased slightly yet significantly compared with baseline value after the meal (p = 0.009; Figure 4D). No differences were observed in plasma triglyceride level after the meal consumption. Plasma triglyceride levels increased significantly after the cold stimulus, while a significant decrease was observed during the negative control (fasting) conditions (Figure 4F). Plasma thyroid-stimulating hormone (TSH), free T3, and free T4 decreased after taking meal (p < 0.05), and plasma TSH and free T3 decreased during cold stimulation and in negative control conditions. However, plasma free T4 slightly increased after cold stimulation, while no difference was seen in negative control conditions (Figures 4G–4I). Skin temperature rose significantly after the meal intake, but no difference was found immediately after the cold stress or during the negative control experiments (Figure 4J).

BAT radiodensity, as measured with Hounsfield units, acts as a marker of BAT stored lipids and tissue retained blood volume (U Din et al., 2017). BAT radiodensity tended to be different after cold stimulus compared with baseline negative control conditions (p = 0.08). However, the cold-stimulated BAT radiodensity was similar to that in postprandial state (p = 0.32; Figure 4K); this is likely because of tissue hyperemia due to hyperperfusion in both states, and it remains unclear whether BAT consumes intracellular lipid in postprandial state.

Insulin acts as a stimulator for BAT glucose uptake (Orava et al., 2011; Vosselman et al., 2013); however, sole insulin elevation may not activate BAT thermogenic mechanism, as Orava et al. (2011) did not find any profound effect of insulin stimulation on BAT blood flow. Our data revealed a link between postprandial plasma adrenaline concentrations and BAT oxygen consumption (r = 0.79, p = 0.01), blood flow (r = 0.83, p = 0.005), and BAT NEFA uptake (r = 0.78, p = 0.002), which signifies the complex interactive mechanism of multiple factors involved in postprandial BAT metabolism. Previously, a role of adrenaline in regulating lipoprotein lipase (Pedersen et al., 1999), adipose tissue capillary recruitment (Tobin et al., 2012), *PGC-1α*, and *UCP1* (Sharara-Chami et al., 2010) has been proposed, and based on our data we speculate that adrenaline may act as a BAT metabolic regulator in postprandial state, although further mechanistic studies are required.

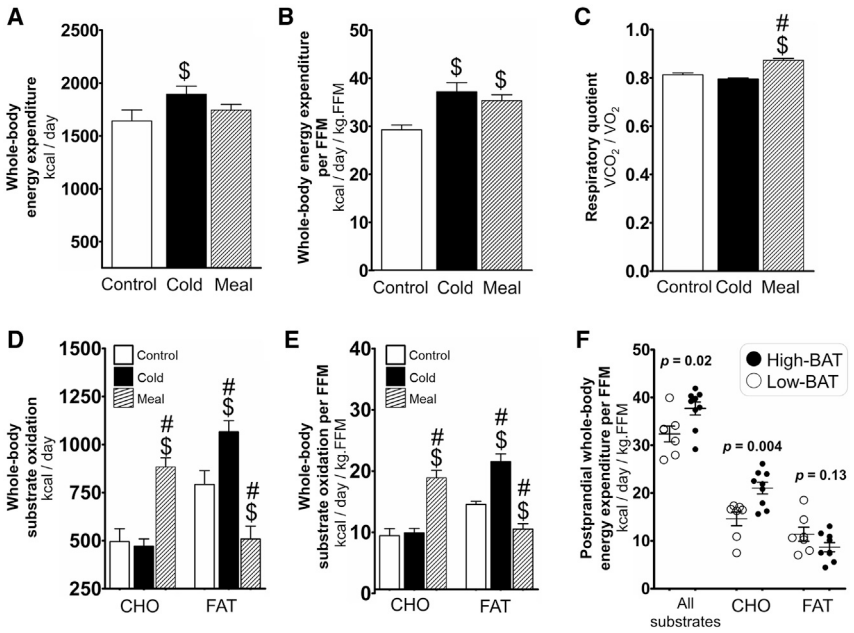

Figure 3. Whole-Body EE Measurements

(A) Whole-body EE at control conditions, during mild cold stress, and after meal intake, measured with indirect calorimeter.

(B) Whole-body EE per kilogram of lean body mass (FFM).

(C) RQs.

(D) Whole-body substrate oxidation.

(E) Whole-body substrate oxidation per kilogram of lean body mass (FFM).

(F) Differences in postprandial EE (per kilogram of lean body mass) and substrate oxidation rates (per kilogram of lean body mass) in high-BAT and low-BAT subjects. Error bars represent ± SEM.

CHO, carbohydrate; High-BAT, subjects with cold-stimulated BAT NEFA uptake $\geq$0.7 μmol/100 g/min; Low-BAT, <0.7 μmol/100 g/min. $, significantly different from negative control ($p < 0.05$). #, significant difference between cold and meal measurements ($p < 0.05$).

Gene Expression in BAT and WAT in Postprandial State

In the postprandial state, the net influx rate of [^{18}F]FTHA was elevated into BAT, whereas the mean total NEFA uptake was decreased, due to a meal-induced reduction in circulating NEFA levels. Despite this decrease in the mean total NEFA uptake, regarding the variation between individual subjects, the postprandial oxygen consumption in BAT (thermogenesis) showed a positive correlation with total NEFA uptake into BAT. This observation suggested the existence of an efficient mechanism mediating the uptake, metabolism, and storage of fatty acids to support meal-induced thermogenesis in BAT. In order to identify the mediators involved, we performed next-generation transcriptome sequencing with paired BAT and WAT biopsies obtained from the supraclavicular region of an independent study cohort. The anthropometric characteristics of this study cohort are shown in Table S1.

UCP1 was expressed at higher levels in BAT versus WAT of all subjects, confirming the thermogenic nature of the BAT biopsies. Using the DEseq2 algorithm and Benjamini-Hochberg technique for multiple testing correction (Benjamini and Hochberg, 1995; Love et al., 2014), we identified a total of 463 BAT-enriched genes; i.e., genes with a significantly higher log2-fold expression difference of $\geq$1 in BAT versus WAT. Within this BAT-enriched gene cluster, an explorative pathway analysis revealed 29 biological processes related to lipid metabolism with significantly higher expression of 68 individual genes (Table 2; Figure 5). Among these, the expression of 52 genes significantly correlated with the expression of *UCP1* in BAT, suggesting a causal relationship between postprandial lipid metabolism and meal-induced thermogenesis (Table S2). The protein products of these genes mediate a variety of different functions, including fatty acid beta-oxidation, the synthesis and breakdown of activated fatty acids, acylglycerol formation, phospholipid hydrolysis, oxylipin synthesis, and mitochondrial energy turnover, for instance, indicating the occurrence of anabolic, catabolic, and regulatory lipid turnover. Thus, the fate of internalized lipids during postprandial thermogenesis currently remains elusive and requires further investigation.

In line with a recent study (Lasar et al., 2018), we identified glycerol kinase (GK) as a gene expressed at higher levels in human BAT versus WAT and strongly correlated with *UCP1* expression (Table S2). Beyond the study of Lasar and colleagues (2018), we observed strong correlations between the expression of *UCP1* and a large number of further genes involved in lipid metabolism, including 3-hydroxy-3-methylglutaryl-CoA synthase 2 (mitochondrial) (HMGCS2), succinate-CoA ligase ADP-forming beta subunit (SUCLA2), succinate dehydrogenase complex iron sulfur subunit B (SDHB), pantothenate kinase 1 (PANK1), PPARG coactivator 1 beta (PPARGC1B), arginase 2 (ARG2), cytochrome P450 family 2 subfamily C member 19 (CYP2C19), lipase family member J (LIPJ), and phosphatidylinositol-4-phosphate 5-kinase type 1 beta (PIP5K1B) (Table S2). Inter-individual differences in *UCP1* expression of BAT were best reflected by these genes (Figure 5), suggesting their encoded proteins as strong candidates for a putative, functional contribution to BAT-mediated postprandial thermogenesis.

Following their uptake into brown adipocytes, de novo triglyceride synthesis has been proposed as the main pathway of NEFA utilization serving the replenishment of thermogenic substrates preceding their subsequent utilization via lipolytic pathways (Labbé et al., 2015). The GK enzyme initiates triglyceride synthesis by the phosphorylation of glycerol. Thus, NEFA uptake into BAT in postprandial state may serve to fuel meal-induced thermogenesis, and GK (besides other candidates) may represent a crucial mediator of this process. Additionally, circulating NEFAs may act as physiological activators of *UCP1*, as indicated previously (Marette and Bukowiecki, 1991). However, the method of the assessment of NEFA uptake into BAT using [^{18}F]FTHA PET radiotracer cannot assess the uptake of those NEFAs that are released from the chylomicrons by the activity of lipoprotein lipase (LPL) locally at the brown adipocytes. Rodent studies suggest that insulin activates LPL in adipose

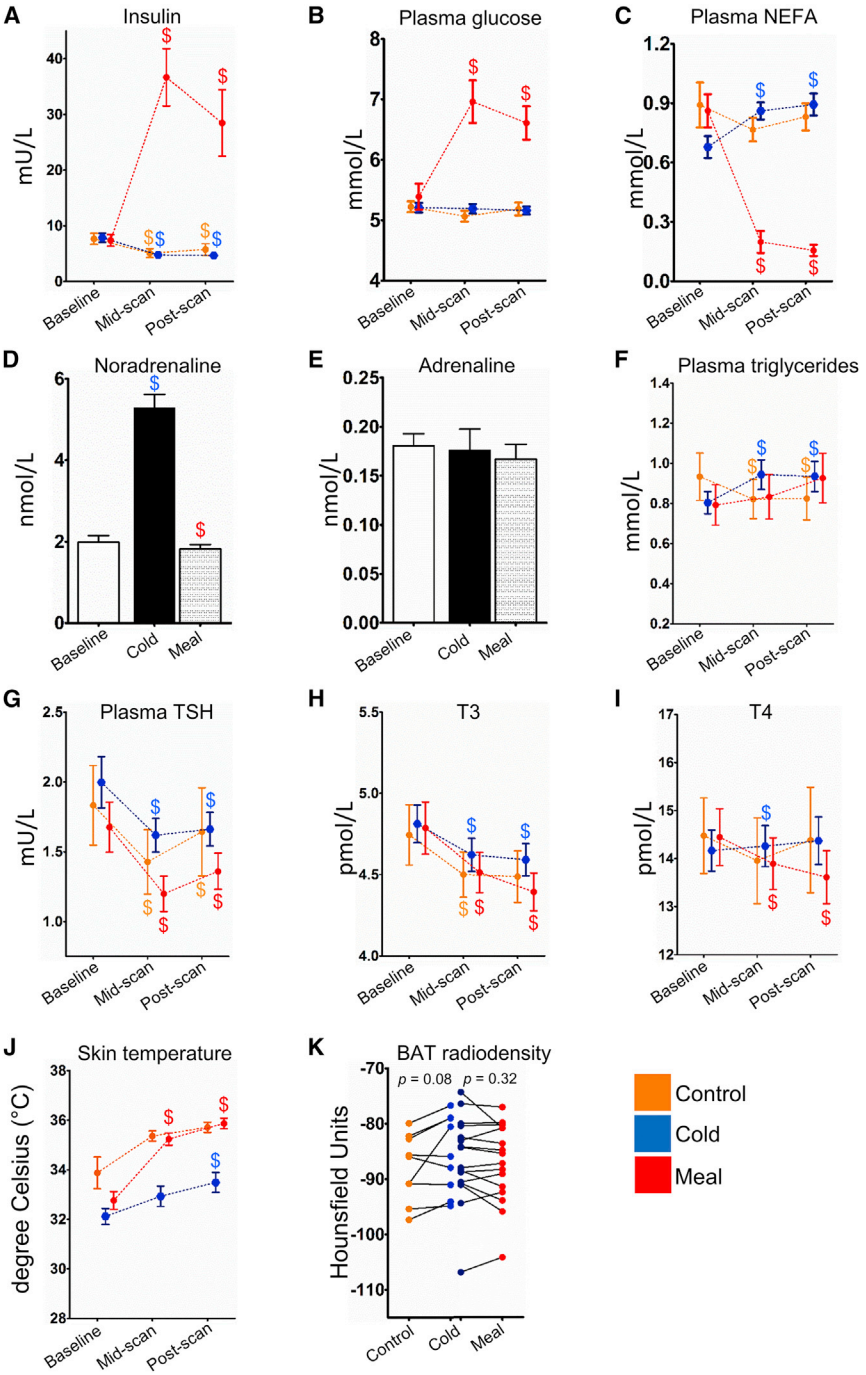

Figure 4. Hormones, Metabolites, Skin Temperature, and BAT Composition Measurements

Hormones (A, D, E, and G–I), metabolites (B, C, and F), skin temperature (J), and BAT radiodensity (K) measured at different time points. Blue color represents measurements during cold stimulus, red color shows the measurements performed during meal experimental sessions, and orange color shows measurement of control group during the fasting-room temperature experiments. Error bars represent ±SEM. $, significantly different from paired baseline measurement ($p < 0.05$).

tissues, including BAT (Kersten, 2014; Wang and Eckel, 2009). It is possible that these LPL-derived NEFAs contribute extensively as a substrate for postprandial BAT thermogenesis, though this pathway in humans is difficult to assess with the current methods.

Postprandial BAT Metabolism in Relation to Whole Body

The tissue-specific oxygen consumption measurements allow estimation of the tissue potential in energy dissipation (Muzik et al., 2013; U Din et al., 2016). Since BAT oxygen consumption in postprandial state is higher than the surrounding muscles and WAT (Figure 2), BAT has substantial comparative postprandial energy dissipation ability. Based on previous evidence and calculations in this study (Table 1), however, the total BAT quantity in the human cervicothoracic region may merely range up to 300 g (Chen et al., 2013; Gerngroß et al., 2017; van Marken Lichtenbelt et al., 2009; Orava et al., 2011; U Din et al., 2016), while muscles and WAT constitute the major volume, contributing BAT as a minor energy-dissipating tissue in the whole scenario. We estimated based on our current measurements that BAT may contribute 13 ± 8 (range: 3–28) kcal of energy per day per 100 g of the available tissue in postprandial state, which is similar to that of during cold stimulation, and reported earlier as well (U Din et al., 2016). Though 13 ± 8 kcal per 100 g per day may appear a modest energy quantity, extrapolating the maximum observed amount (28 kcal/100 g/day) to the whole calendar year will yield approximately 25.5 thousand kilocalories in an individual possessing merely 250 g of BAT. This amount of energy consumption is almost equivalent to burning 3.4 kg fat (87% lipid). Of note, BAT is likely not active for the entire 24 hr in a day; however, we are in postprandial state for most of the awake time. Thus, recruiting additional brown adipocytes and maintaining the functional activity may still be one of the viable options for whole-body weight management. Accordingly, BAT postprandial circulatory NEFA uptake was almost 2-fold higher than muscles and WAT, yet it may represent merely a minor proportional total systemic uptake (Blondin et al., 2017) owing to limited BAT volume in an adult human body; nevertheless, the total potential of the perpetually activated tissue in systemic lipid clearance cannot be ruled out.

Postprandial BAT oxygen consumption correlates inversely with waist circumference ($r = -0.75$, $p = 0.01$) in the current

Table 2. BAT-Enriched Biological Processes Related to Lipid Metabolism

Biological Process	Regulated Genes	Genes in Pathway	p Value (−log10)
Monocarboxylic acid metabolic process	32	459	6.78
Carboxylic acid metabolic process	49	896	6.74
Organic acid metabolic process	50	1,025	5.41
Fatty acid metabolic process	21	325	4.15
Lipid metabolic process	48	1,187	3.21
Organic acid catabolic process	14	204	3.20
Carboxylic acid catabolic process	14	204	3.20
Cellular lipid metabolic process	38	878	3.17
Dicarboxylic acid metabolic process	8	80	3.07
Long-chain fatty acid metabolic process	8	82	3.00
Monocarboxylic acid catabolic process	8	91	2.71
Fatty acid beta-oxidation	6	57	2.54
Regulation of fatty acid metabolic process	6	70	2.10
Negative regulation of fatty acid metabolic process	3	17	2.09
Fatty acid beta-oxidation using acyl-CoA dehydrogenase	2	6	2.06
Arachidonic acid metabolic process	5	53	2.00
Fatty acid catabolic process	6	74	1.99
Triglyceride biosynthetic process	5	55	1.93
Fatty acid oxidation	6	78	1.88
Acylglycerol biosynthetic process	5	57	1.86
Neutral lipid biosynthetic process	5	57	1.86
Triglyceride metabolic process	7	104	1.81
Lipid oxidation	6	81	1.80
Regulation of lipid metabolic process	11	215	1.71
Acylglycerol metabolic process	7	109	1.71
Neutral lipid metabolic process	7	110	1.69
Positive regulation of fatty acid biosynthetic process	2	13	1.39
Methyl-branched fatty acid metabolic process	1	2	1.31
Lipid modification	7	133	1.31

data; however, a causal relationship for active BAT solely being suppressant of obesity is unlikely, based on minor BAT postprandial thermogenic potential. Additionally, there was an inverse relationship between waist circumference and postprandial oxygen consumption of cervico-thoracic muscles (mean oxygen consumption of cervico-thoracic muscles, $rho = -0.67$, $p = 0.018$); the waist circumference also tended to correlate with oxygen consumption of WAT ($rho = -0.67$, $p = 0.07$). Since muscle and adipose tissue mass constitute a major portion of the human body, this inter-individual variation in postprandial oxygen consumption in muscles and WAT is likely a factor for the development of obesity due to the impaired meal-induced thermogenesis mechanism. There was no obvious relationship of oxygen consumption of BAT, WAT, or muscles with whole-body insulin sensitivity or postprandial plasma insulin concentrations.

We report here that BAT has minor thermogenic contribution to meal-induced thermogenesis; however, it is possible that BAT postprandial thermogenesis, in conjunction with other postprandial thermogenic reactions, could play a role in the regulation of satiety. In humans, meal-induced thermogenesis (Crovetti et al., 1998), and in rodents, BAT thermogenesis (Glick, 1982) have been previously been linked to satiety. Nevertheless, a systematic approach is needed to effectively investigate this phenomenon in humans.

Limitations of the Study

Due to technical aspects and limited FOV of the scanner, the assessment of BAT depots was restricted to cervico-thoracic region only. Additionally, we were not able to perform all three PET/CT scans (cold, fasting/room temperature, and meal-induced) for each participant due to radiation dose limits. Moreover, our current methods cannot clearly discern the mechanism by which circulating NEFAs taken up by BAT contribute to postprandial thermogenesis.

Conclusions

A single meal, dominant in carbohydrates and comprising all macronutrients, can stimulate BAT thermogenesis. Although human cervico-thoracic BAT appears to have a minor thermogenic potential compared with whole-body thermogenesis in postprandial state, the magnitude of BAT postprandial thermogenesis is almost equivalent to cold activation. The mechanism of

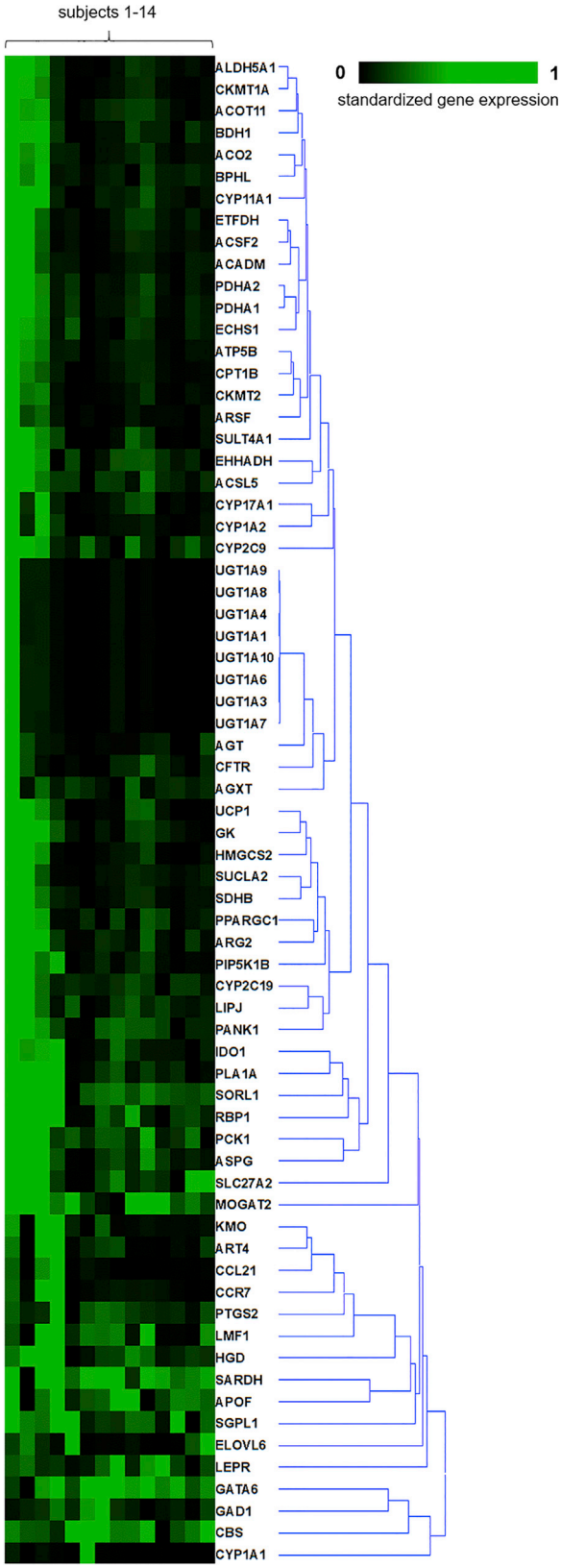

Figure 5. Heatmap Illustrating Gene Expression of Uncoupling Protein 1 (*UCP1*) and 68 Additional Genes Related to Lipid Metabolism in Supraclavicular BAT of 14 Subjects

Columns represent individual subjects. The inter-individual range of gene expression values (reads per kilobase per million mapped reads, RPKM) was standardized for each gene to be displayed as values between 0 (black) and 1 (green), indicating low/absent or high expression, respectively. The arrangement of genes is based on hierarchical clustering. All displayed genes are enriched in BAT versus WAT as defined by a significant adjusted $p \leq 0.05$, calculated with the DESeq2 algorithm and Benjamini-Hochberg technique for multiple testing correction (Benjamini and Hochberg, 1995; Love et al., 2014) log2-fold gene expression difference of ≥ 1.

BAT activation and substrate utilization in postprandial state, compared with cold stimulus, appears to be different. A number of genes participating in lipid metabolism pathways are significantly correlated with *UCP1* expression in human BAT, some of which may represent crucial mediators of meal-induced thermogenesis. In postprandial state, contribution of non-LPL-derived circulating NEFAs appears to be minimal and insulin has a dominant effect on substrate utilization.

STAR★METHODS

Detailed methods are provided in the online version of this paper and include the following:

- KEY RESOURCES TABLE
- CONTACT FOR REAGENT AND RESOURCE SHARING
- EXPERIMENTAL MODEL AND SUBJECT DETAILS
  - Study Subjects
  - Study Design
- METHOD DETAILS
  - Scanning Protocol, PET Image Reconstruction and Data Analysis
  - Indirect Respiratory Calorimetry
  - Adipose Tissue Biopsies, RNA Isolation and Next Generation Sequencing
- QUANTIFICATION AND STATISTICAL ANALYSIS
- DATA AND SOFTWARE AVAILABILITY
- ADDITIONAL RESOURCES

SUPPLEMENTAL INFORMATION

Supplemental Information includes three figures and three tables and can be found with this article online at https://doi.org/10.1016/j.cmet.2018.05.020.

ACKNOWLEDGMENTS

The authors thank the staff of the Turku PET Center for their technical assistance. Tarja Niemi and Markku Taittonen are acknowledged for their crucial role in taking human BAT and WAT biopsies. The study was financially supported by Academy of Finland (259926, 265204, 292839, and 269977), the Paulo Foundation, the Finnish Cultural Foundation Southwest Finland Regional Fund, the Turku University Hospital Research Funds, the European Union (EU FP7 project 278373; DIABAT), and a joint French/German grant ANR/DFG (Nutribrite). The study was conducted within the Finnish Center of Excellence in Cardiovascular and Metabolic Diseases supported by the Academy of Finland, University of Turku, Turku University Hospital, and Åbo Akademi University.

AUTHOR CONTRIBUTIONS

M.U.D. and T.S. drafted the manuscript, and analyzed and interpreted the image data. J.R. contributed to acquiring and interpreting the scanning data. The

role of N.K. was crucial in mathematical modeling of dynamic PET data. M.L. contributed to acquiring the tissue samples for the gene analyses. S.F.M., T.F., E.-Z.A., and M.K. provided the gene expression data and commented on the manuscript draft. O.S. was responsible for production of PET tracers. P.N. and K.A.V. contributed to the conception and design, revising, enhancing intellectual content, and approving the final edition of the manuscript.

DECLARATION OF INTERESTS

The authors declare no competing interests.

Received: November 15, 2016
Revised: October 31, 2017
Accepted: May 22, 2018
Published: June 14, 2018

REFERENCES

Allard, M., and Leblanc, J. (1988). Effects of cold acclimation, cold exposure, and palatability on postprandial thermogenesis in rats. Int. J. Obes. *12*, 169–178.

Benjamini, Y., and Hochberg, Y. (1995). Controlling the false discovery rate: a practical and powerful approach to multiple testing. J. R. Stat. Soc. Ser. B *57*, 289–300.

Blondin, D.P., Tingelstad, H.C., Noll, C., Frisch, F., Phoenix, S., Guérin, B., Turcotte, É.E., Richard, D., Haman, F., and Carpentier, A.C. (2017). Dietary fatty acid metabolism of brown adipose tissue in cold-acclimated men. Nat. Commun. *8*, 14146.

Chen, K.Y., Brychta, R.J., Linderman, J.D., Smith, S., Courville, A., Dieckmann, W., Herscovitch, P., Millo, C.M., Remaley, A., Lee, P., et al. (2013). Brown fat activation mediates cold-induced thermogenesis in adult humans in response to a mild decrease in ambient temperature. J. Clin. Endocrinol. Metab. *98*, 1218–1223.

Crovetti, R., Porrini, M., Santangelo, A., and Testolin, G. (1998). The influence of thermic effect of food on satiety. Eur. J. Clin. Nutr. *52*, 482–488.

Feldmann, H.M., Golozoubova, V., Cannon, B., and Nedergaard, J. (2009). UCP1 ablation induces obesity and abolishes diet-induced thermogenesis in mice exempt from thermal stress by living at thermoneutrality. Cell Metab. *9*, 203–209.

Gerngroß, C., Schretter, J., Klingenspor, M., Schwaiger, M., and Fromme, T. (2017). Active brown fat during ^{18}F-FDG PET/CT imaging defines a patient group with characteristic traits and an increased probability of brown fat redetection. J. Nucl. Med. *58*, 1104–1110.

Glick, Z. (1982). Inverse relationship between brown fat thermogenesis and meal size: the thermostatic control of food intake revisited. Physiol. Behav. *29*, 1137–1140.

Glick, Z., and Raum, W.J. (1986). Norepinephrine turnover in brown adipose tissue is stimulated by a single meal. Am. J. Physiol. *251*, R13–R17.

Glick, Z., Teague, R., and Bray, G. (1981). Brown adipose tissue: thermic response increased by a single low protein, high carbohydrate meal. Science *213*, 1125–1127.

Glick, Z., Teague, R.J., Bray, G.A., and Lee, M. (1983). Compositional and metabolic changes in brown adipose tissue following a single test meal. Metabolism *32*, 1146–1150.

Glick, Z., Wickler, S.J., Stern, J.S., and Horwitz, B.A. (1984). Regional blood flow in rats after a single low-protein, high-carbohydrate test meal. Am. J. Physiol. *247*, R160–R166.

Glick, Z., Wu, S.Y., Lupien, J., Reggio, R., Bray, G.A., and Fisher, D.A. (1985). Meal-induced brown fat thermogenesis and thyroid hormone metabolism in rats. Am. J. Physiol. *249*, E519–E524.

Hibi, M., Oishi, S., Matsushita, M., Yoneshiro, T., Yamaguchi, T., Usui, C., Yasunaga, K., Katsuragi, Y., Kubota, K., Tanaka, S., et al. (2016). Brown adipose tissue is involved in diet-induced thermogenesis and whole-body fat utilization in healthy humans. Int. J. Obes. *40*, 1655–1661.

Himms-Hagen, J. (1984). Nonshivering thermogenesis. Brain Res. Bull. *12*, 151–160.

Kersten, S. (2014). Physiological regulation of lipoprotein lipase. Biochim. Biophys. Acta *1841*, 919–933.

Kontani, Y., Wang, Y., Kimura, K., Inokuma, K.-I., Saito, M., Suzuki-Miura, T., Wang, Z., Sato, Y., Mori, N., and Yamashita, H. (2005). UCP1 deficiency increases susceptibility to diet-induced obesity with age. Aging Cell *4*, 147–155.

Kozak, L.P. (2010). Brown fat and the myth of diet-induced thermogenesis. Cell Metab. *11*, 263–267.

Kudomi, N., Hirano, Y., Koshino, K., Hayashi, T., Watabe, H., Fukushima, K., Moriwaki, H., Teramoto, N., Iihara, K., and Iida, H. (2013). Rapid quantitative CBF and CMRO(2) measurements from a single PET scan with sequential administration of dual (15)O-labeled tracers. J. Cereb. Blood Flow Metab. *33*, 440–448.

Labbé, S.M., Caron, A., Bakan, I., Laplante, M., Carpentier, A.C., Lecomte, R., and Richard, D. (2015). In vivo measurement of energy substrate contribution to cold-induced brown adipose tissue thermogenesis. FASEB J. *29*, 2046–2058.

Lasar, D., Rosenwald, M., Kiehlmann, E., Balaz, M., Tall, B., Opitz, L., Lidell, M.E., Zamboni, N., Krznar, P., Sun, W., et al. (2018). Peroxisome proliferator activated receptor gamma controls mature brown adipocyte inducibility through glycerol kinase. Cell Rep. *22*, 760–773.

Liu, X., Rossmeisl, M., McClaine, J., Kozak, L.P., Harper, M.-E., and Kozak, L.P. (2003). Paradoxical resistance to diet-induced obesity in UCP1-deficient mice. J. Clin. Invest. *111*, 399–407.

Love, M.I., Huber, W., and Anders, S. (2014). Moderated estimation of fold change and dispersion for RNA-seq data with DESeq2. Genome Biol. *15*, 550.

Lupien, J.R., Glick, Z., Saito, M., and Bray, G.A. (1985). Guanosine diphosphate binding to brown adipose tissue mitochondria is increased after single meal. Am. J. Physiol. *249*, R694–R698.

Ma, S.W.Y., and Foster, D.O. (1986). Uptake of glucose and release of fatty acids and glycerol by rat brown adipose tissue *in vivo*. Can. J. Physiol. Pharmacol. *64*, 609–614.

Marette, A., and Bukowiecki, L.J. (1991). Noradrenaline stimulates glucose transport in rat brown adipocytes by activating thermogenesis. Evidence that fatty acid activation of mitochondrial respiration enhances glucose transport. Biochem. J. *277* (Pt 1), 119–124.

Meriläinen, P.T. (1987). Metabolic monitor. Int. J. Clin. Monit. Comput. *4*, 167–177.

Muzik, O., Mangner, T.J., Leonard, W.R., Kumar, A., Janisse, J., and Granneman, J.G. (2013). 15O PET measurement of blood flow and oxygen consumption in cold-activated human brown fat. J. Nucl. Med. *54*, 523–531.

Nedergaard, J., Golozoubova, V., Matthias, A., Asadi, A., Jacobsson, A., and Cannon, B. (2001). UCP1: the only protein able to mediate adaptive non-shivering thermogenesis and metabolic inefficiency. Biochim. Biophys. Acta *1504*, 82–106.

Nuutila, P., Peltoniemi, P., Oikonen, V., Larmola, K., Kemppainen, J., Takala, T., Sipilä, H., Oksanen, A., Ruotsalainen, U., Bolli, G.B., et al. (2000). Enhanced stimulation of glucose uptake by insulin increases exercise-stimulated glucose uptake in skeletal muscle in humans: studies using [15O]O2, [15O]H2O, [18F]fluoro-deoxy-glucose, and positron emission tomography. Diabetes *49*, 1084–1091.

Oikonen, V., Nuutila, P., Sipilä, H., Tolvanen, T., Peltoniemi, P., and Ruotsalainen, U. (1998). Quantification of oxygen consumption in skeletal muscle with PET and oxygen-15 bolus. Eur. J. Nucl. Med. *25*, 1151.

Olsen, J.M., Csikasz, R.I., Dehvari, N., Lu, L., Sandström, A., Öberg, A.I., Nedergaard, J., Stone-Elander, S., and Bengtsson, T. (2017). β3-Adrenergically induced glucose uptake in brown adipose tissue is independent of UCP1 presence or activity: mediation through the mTOR pathway. Mol. Metab. *6*, 611–619.

Orava, J., Nuutila, P., Lidell, M.E., Oikonen, V., Noponen, T., Viljanen, T., Scheinin, M., Taittonen, M., Niemi, T., Enerbäck, S., et al. (2011). Different metabolic responses of human brown adipose tissue to activation by cold and insulin. Cell Metab. *14*, 272–279.

Orava, J., Nuutila, P., Noponen, T., Parkkola, R., Viljanen, T., Enerbäck, S., Rissanen, A., Pietiläinen, K.H., and Virtanen, K.A. (2013). Blunted metabolic responses to cold and insulin stimulation in brown adipose tissue of obese humans. Obesity *21*, 2279–2287.

Ouellet, V., Labbé, S.M., Blondin, D.P., Phoenix, S., Guérin, B., Haman, F., Turcotte, E.E., Richard, D., and Carpentier, A.C. (2012). Brown adipose tissue oxidative metabolism contributes to energy expenditure during acute cold exposure in humans. J. Clin. Invest. *122*, 545–552.

Patlak, C.S., and Blasberg, R.G. (1985). Graphical evaluation of blood-to-brain transfer constants from multiple-time uptake data. Generalizations. J. Cereb. Blood Flow Metab. *5*, 584–590.

Pedersen, S.B., Bak, J.F., Holck, P., Schmitz, O., and Richelsen, B. (1999). Epinephrine stimulates human muscle lipoprotein lipase activity in vivo. Metabolism *48*, 461–464.

Peterson, C.M., Orooji, M., Johnson, D.N., Naraghi-Pour, M., and Ravussin, E. (2017). Brown adipose tissue does not seem to mediate metabolic adaptation to overfeeding in men. Obesity *25*, 502–505.

Rothwell, N.J., and Stock, M.J. (1979). A role for brown adipose tissue in diet-induced thermogenesis. Nature *281*, 31–35.

Savisto, N., Viljanen, T., Kokkomäki, E., Bergman, J., and Solin, O. (2018). Automated production of [^{18}F]FTHA according to GMP. J. Labelled Comp. Radiopharm. *61*, 84–93.

Sharara-Chami, R.I., Joachim, M., Mulcahey, M., Ebert, S., and Majzoub, J.A. (2010). Effect of epinephrine deficiency on cold tolerance and on brown adipose tissue. Mol. Cell. Endocrinol. *328*, 34–39.

Strijckmans, K., Vandecasteele, C., and Sambre, J. (1985). Production and quality control of 15O2 and C15O2 for medical use. Int. J. Appl. Radiat. Isot. *36*, 279–283.

Tappy, L. (1996). Thermic effect of food and sympathetic nervous system activity in humans. Reprod. Nutr. Dev. *36*, 391–397.

Tentolouris, N., Alexiadou, K., Kokkinos, A., Koukou, E., Perrea, D., Kyriaki, D., and Katsilambros, N. (2011). Meal-induced thermogenesis and macronutrient oxidation in lean and obese women after consumption of carbohydrate-rich and fat-rich meals. Nutrition *27*, 310–315.

Tobin, L., Simonsen, L., Galbo, H., and Bulow, J. (2012). Vascular and metabolic effects of adrenaline in adipose tissue in type 2 diabetes. Nutr. Diabetes *2*, e46.

U Din, M., Raiko, J., Saari, T., Kudomi, N., Tolvanen, T., Oikonen, V., Teuho, J., Sipilä, H.T., Savisto, N., Parkkola, R., et al. (2016). Human brown adipose tissue [15O]O2 PET imaging in the presence and absence of cold stimulus. Eur. J. Nucl. Med. Mol. Imaging *43*, 1878–1886.

U Din, M., Raiko, J., Saari, T., Saunavaara, V., Kudomi, N., Solin, O., Parkkola, R., Nuutila, P., and Virtanen, K.A. (2017). Human brown fat radiodensity indicates underlying tissue composition and systemic metabolic health. J. Clin. Endocrinol. Metab. *102*, 2258–2267.

van Marken Lichtenbelt, W.D., Vanhommerig, J.W., Smulders, N.M., Drossaerts, J.M.A.F.L., Kemerink, G.J., Bouvy, N.D., Schrauwen, P., and Teule, G.J.J. (2009). Cold-activated brown adipose tissue in healthy men. N. Engl. J. Med. *360*, 1500–1508.

Virtanen, K.A., Lidell, M.E., Orava, J., Heglind, M., Westergren, R., Niemi, T., Taittonen, M., Laine, J., Savisto, N.-J., Enerbäck, S., et al. (2009). Functional brown adipose tissue in healthy adults. N. Engl. J. Med. *360*, 1518–1525.

Vosselman, M.J., Brans, B., Van Der Lans, A.A.J.J., Wierts, R., Van Baak, M.A., Mottaghy, F.M., Schrauwen, P., and Van Marken Lichtenbelt, W.D. (2013). Brown adipose tissue activity after a high-calorie meal in humans. Am. J. Clin. Nutr. *98*, 57–64.

Vrieze, A., Schopman, J.E., Admiraal, W.M., Soeters, M.R., Nieuwdorp, M., Verberne, H.J., and Holleman, F. (2012). Fasting and postprandial activity of brown adipose tissue in healthy men. J. Nucl. Med. *53*, 1407–1410.

Wang, H., and Eckel, R.H. (2009). Lipoprotein lipase: from gene to obesity. Am. J. Physiol. Metab. *297*, E271–E288.

Weir, J.B. (1949). New methods for calculating metabolic rate with special reference to protein metabolism. J. Physiol. *109*, 1–9.

Westerterp, K.R., Wilson, S.A., and Rolland, V. (1999). Diet induced thermogenesis measured over 24h in a respiration chamber: effect of diet composition. Int. J. Obes. Relat. Metab. Disord. *23*, 287–292.

Yoneshiro, T., Aita, S., Matsushita, M., Kameya, T., Nakada, K., Kawai, Y., and Saito, M. (2011). Brown adipose tissue, whole-body energy expenditure, and thermogenesis in healthy adult men. Obesity *19*, 13–16.

STAR★METHODS

KEY RESOURCES TABLE

REAGENT or RESOURCE	SOURCE	IDENTIFIER
Biological Samples		
Human supraclavicular white adipose tissue	Turku PET Centre, Turku University Hospital	http://turkupetcentre.fi/
Human supraclavicular brown adipose tissue	Turku PET Centre, Turku University Hospital	http://turkupetcentre.fi/
Human blood samples (serum and plasma)	Turku PET Centre, Turku University Hospital	http://turkupetcentre.fi/
Critical Commercial Assays		
TruSeq RNA Access Coding Transcriptome	Illumina	Cat# RS-301-2001
Deposited Data		
RNA-Seq data	Tissue samples from this study	GEO: GSE113764
Software and Algorithms		
Carimas, PET-CT image data analysis software	Turku PET Centre	http://turkupetcentre.fi/carimas/
IBM SPSS Statistics 22	IBM	RRID: SCR_002865
GraphPad Prism 7	GraphPad Software	RRID: SCR_002798
Genomatix	Genomatix AG	RRID: SCR_008036
Hierarchical Clustering Explorer 3.5	Human Computer Interaction Lab	http://www.cs.umd.edu/hcil/hce/
Other		
[^{15}O]O_2, radiotracer	Turku PET Centre radiochemistry	http://turkupetcentre.fi/radiochemistry/
[^{15}O]H_2O, radiotracer	Turku PET Centre, Hidex Radiowater Generator	http://turkupetcentre.fi/radiochemistry/, http://hidex.com/
[^{18}F]FTHA, radiotracer	Turku PET Centre radiochemistry	http://turkupetcentre.fi/radiochemistry/
Deltatrac II, indirect respiratory calorimetry	Datex-Ohmeda	N/A
Blanketrol III (cooling blanket)	Cincinnati Sub-Zero	https://www.cszmedical.com/blanketrol-iii
Discovery 690 PET-CT scanner	General Electric Medical Systems	http://www3.gehealthcare.com/en/education/product_education_clinical/tip_applications/pet_onsite/discovery_pet-ct_690

CONTACT FOR REAGENT AND RESOURCE SHARING

Further information and requests for resources and reagents should be directed to and will be fulfilled by the Lead Contact, Kirsi Virtanen (kirsi.virtanen@utu.fi).

EXPERIMENTAL MODEL AND SUBJECT DETAILS

Study Subjects

Healthy lean and obese volunteers (n = 25) of both sexes (16 females and 9 males) participated in the study with the approval of ethical review board of the Hospital District of Southwest Finland. All enrolled study subjects were non-diabetic, had normal oral glucose tolerance test, healthy cardiovascular status and level of circulatory hepatic enzymes within adequate range. Informed written consent was obtained from all study subjects prior to inclusion in the study. The study was carried out according to the principles of declaration of Helsinki and GCP guidelines. The subjects were divided into experimental group (n = 16, 12 females and 4 males, mean age 35.4 ± 11.3) and control group (n = 9, 4 females and 5 males, mean age 36.3 ± 9.3). There were no significant differences in anthropometric characteristics between these two groups (Table 1). Among the nine control group subjects, [^{15}O]O_2 scans was conducted for seven subjects, while [^{18}F]FTHA scans were performed for all nine subjects. The data of the control experiments (seven subjects) has been reported in a previous study (U Din et al., 2016).

Study Design

Participants underwent scanning sessions which only differed by external stimuli; the experimental group was scanned at two different known thermogenic physiological conditions, cold and after taking a meal (Figure 1), while the control group underwent scanning with cold stimulus (positive control) and without cold stimulus at room temperature of ~22°C (negative control). Each subject participated in two scanning sessions which were organized on two different days, while the minimum duration between the two sessions was one week. In all scanning sessions, subjects were fasted overnight and scans were performed at the same time of the day in order to minimize any possible effects of the individual circadian rhythms on body metabolism. In cold stimulus experiments, subjects were given cold stimulus using cooling blankets for two hours prior to the start of the scan and cold stimulus continued during the scans as well (U Din et al., 2016). In standardised-meal experiments, subjects ingested a meal of approximately 542 kcal, of which 58 % were carbohydrates, while 25% and 17% belonged to fats and proteins, respectively. The detailed contents of the meal are provided in Table S3. The subjects finished the meal ingestion in approximately 15 minutes, and following 15 minutes from the ingestion the scanning was initiated. The skin temperature of the subjects was also monitored during scanning using a digital thermometer (Art.183, Termometerfabriken Viking AB, Eskilstuna, Sweden) while the temperature sensing probe attached to the lateral abdominal skin surface. Cold stimulus experiment readings acted as paired positive control, while the experiments at room temperature acted as negative control for the postprandial experiment measurements. The scanning sessions were conducted in a random order, regardless of the outdoor temperature, and irrespective of the participant belonging to either the control or experimental group.

METHOD DETAILS

Scanning Protocol, PET Image Reconstruction and Data Analysis

Subjects were placed supine in a head first position inside the PET-CT scanner (Discovery 690 PET-CT scanner; General Electric Medical Systems, Milwaukee, WI, USA; PET voxel size = 3.64 x 3.64 x 3.27 mm), while the level of the clavicles was set to be the centre of the axial field of view (AFOV). Comfortable, relaxed position of the subjects was ensured in order to avoid any tension in the neck muscles, and the arms were placed next to the body. The positioning of the subjects within the scanner was kept identical irrespective the cooling protocol utilised. Scanning started with an attenuation correction transmission CT scan followed by three separate dynamic emission PET scans using three different radiotracers, i.e. [^{15}O]O_2, [^{15}O]H_2O, and [^{18}F]FTHA. In the [^{15}O]O_2 scans, the subjects were given radioactive oxygen gas (509 ± 37 MBq) using a plastic mask with a single deep inhalation and scanning was started simultaneously; 20 frames of variable lengths were acquired over a period of 7 min (frames: 6 × 5 s, 6 × 15 s, 6 × 30 s, 2 × 60 s). Low-energy deuteron accelerator Cyclone 3 (Ion Beam Application, Louvain-la-Neuve, Belgium) was used for the production of [^{15}O]O_2. [^{15}O] isotope was produced by the [^{14}N] (d,n) [^{15}O] nuclear reaction on natural nitrogen gas (Strijckmans et al., 1985). After sufficient radioactive decay of [^{15}O]O_2 (approx. 10 min.), [^{15}O]H_2O (493 ± 35 Mbq) was intravenously injected into the left antecubital vein and scanning started immediately using 20 frames with a dynamic acquisition protocol (frames: 6 × 5 s, 6 × 15 s, 6 × 30 s, 2 × 60 s). [^{15}O]H_2O was produced using Hidex Radiowater Generator (Hidex Oy, Turku, Finland).

After [^{15}O]H_2O had sufficiently decayed (i.e. 10 minutes), an intravenous injection of [^{18}F]FTHA was given and a dynamic emission scan was performed (frames: 1 x 60 s, 6 x 30 s, 1 x 60 s, 3 x 300 s, 2 x 600 s) on the same area as with [^{15}O]H_2O. [^{18}F]FTHA was produced as described by Savisto et al. (2018). After the acquisition of scanning data computerized reconstruction was carried out. Quantitative corrections were applied to PET image data, including detector normalization, dead-time, radioactive decay, randoms, attenuation and scatter. Images were reconstructed using iterative 3D-OSEM (GE Vue Point HD-S) reconstruction using 24 subsets and 2 iterations. All images were filtered using 6.4 mm Gaussian post-filter.

PET-CT image data was analysed using Carimas 2.8 software (Turku PET Centre, Finland). Volumes of interest (VOIs) were drawn at the supraclavicular fat depots for BAT, subcutaneous fat at the posterior side of the neck for WAT, and on deltoid, trapezius, levator scapulae, splenius cervicis and pectoralis major regions for muscle. Image derived blood radioactivity was estimated by drawing VOI at the arch of aorta on PET images. Obtained [^{15}O]H_2O tissue time activity curves (TACs) were quantified using one tissue compartment model (1TCM) for the calculation of local tissue blood flow; while tissue specific oxygen consumption was estimated using [^{15}O]O_2 TACs by incorporating blood flow values in 1TCM (Kudomi et al., 2013; U Din et al., 2016). Muscles oxygen consumption was estimated by also taking into account oxygen binding to myoglobin (Nuutila et al., 2000; Oikonen et al., 1998; U Din et al., 2016). Net influx rate (K_i) of [^{18}F]FTHA was calculated from tissue specific TACs obtained from [^{18}F]FTHA PET scans using Patlak model (Patlak and Blasberg, 1985). Image derived plasma input function was corrected for metabolites which were measured from samples acquired during the scanning. Net NEFA uptake was subsequently calculated by multiplying K_i with plasma NEFA concentration measured during the [^{18}F]FTHA PET scanning (time point 2; Figure 1).

Indirect Respiratory Calorimetry

Whole body energy expenditure (EE) and whole body substrate utilization rates were measured using indirect respiratory calorimetry technique (Deltatrac II, Datex-Ohmeda) performed during scanning sessions for approximately 100 - 120 minutes. Measurements were excluded from analyses if they deviated more than 1.5 SD from the mean vO_2, vCO_2, EE or respiratory quotient values, caused by irregular breathing. The first 30 minutes of the calorimetry data was also excluded. Whole body energy expenditure, respiratory quotient and substrate utilization rates were calculated using vO_2 and vCO_2 according to Weir equation (Weir, 1949) and manufacturer's equations (Meriläinen, 1987) using Matlab (Version: R2011a). Protein oxidation was accounted for in the equations by considering urinary nitrogen to be 13 g/24 h. Whole body energy expenditure and substrate oxidation rates were divided by

fat-free mass in order to compare different subjects; the percentage fat (%) was measured with a bioimpedance based method (Omron BF400, Omron Healthcare).

Adipose Tissue Biopsies, RNA Isolation and Next Generation Sequencing

Paired biopsies of BAT and WAT were obtained from the supraclavicular region of 14 healthy subjects of an independent cohort (Table S1). These subjects had previously participated in other research projects at our institute. The site of the biopsy was determined by any available prior imaging data of the supraclavicular region (for example, MRI, cold exposed [^{18}F]FDG PET, or cold exposed [^{18}F]FTHA PET imaging). The subjects ingested a meal prior to the biopsy procedure. The procedure was carried out at room temperature ($\sim$ 22°C) under local lidocaine-epinephrine anesthesia by a plastic surgeon. The WAT sample was collected from the same incision. The adipose tissue samples were snap-frozen in liquid nitrogen immediately after the excision.

Deep-frozen adipose tissues (approx. 30-120 mg) were homogenized in 1 mL TRIsure (Bioline, London/UK) using a dispersing instrument (Ultra-Turrax D-1, Miccra GmbH, Mühlheim/Germany). RNA was prepared, further purified by spin columns (SV Total RNA Isolation System, Promega, Fitchburg WI/USA) and finally eluted in 50 μL water. The RNA concentration was determined photometrically (Nanodrop ND-1000, Peqlab, Erlangen/Germany). Samples were diluted to a concentration of 25-500 ng/μL, denatured for 2 min at 70°C and RNA integrity determined (Bioanalyzer 2100, Agilent Technologies, Santa Clara CA/USA). The RNA integrity number was not determinable in 1 out of 28 samples and ranged from 3.1 to 8.7 in all other samples. The percentage of fragments with >200 nucleotides (DV200) ranged from 60% to 96%. Accordingly, sequencing libraries were prepared by enriching coding RNA to efficiently compensate for degradation (TruSeq RNA Access Coding Transcriptome, RS-301-2001, Illumina San Diego CA/USA). Libraries were sequenced (HiSeq 2500, Illumina) employing appropriate consumables (HiSeq SBS Kit v4, HiSeq SR Cluster Kit v4, Illumina) to a very high depth of 30.2-160.2 million reads per sample. Reads were mapped by a dedicated software platform (Genome Mining Station, Genomatix München/Germany) resulting in 21.2-111.7 uniquely mapped, coding reads and further analyzed (Genome Analyzer, Genomatix). Differential gene expression was analyzed with the DESeq2 algorithm, which applies the Benjamini-Hochberg technique for multiple testing correction to compute adjusted p-values (Benjamini and Hochberg, 1995; Love et al., 2014). BAT-enriched genes were identified by a significant ($p \leq 0.05$) log2-fold expression difference of ≥ 1 in BAT versus WAT. Biological processes (GO terms) related to lipid metabolism were extracted by an explorative pathway analysis of the BAT-enriched gene cluster using defined keywords (lipid, lipo, fatty acid, organic acid, carboxylic acid, triglyceride, glycero, acyl, phosphor; Pathway System, Genomatix). BAT expression levels ('reads per 1kb transcript length per million mapped reads', RPKM) of significantly regulated genes of these pathways were standardized and illustrated as heatmap (Hierarchical Clustering Explorer 3.5, Human Computer Interaction Lab Maryland/USA). Genes were hierarchically clustered by the Euclidean distance method. R^2 was calculated from the Pearson correlation coefficient to explore the relationship between expression of the uncoupling protein 1 gene and genes of the BAT-enriched gene cluster related to lipid metabolism pathways.

QUANTIFICATION AND STATISTICAL ANALYSIS

Statistical analyses were performed using IBM SPSS Statistics (version 22) and GraphPad Prism. Comparison of means was performed with two-way Student's t-test (negative control vs. meal: unpaired t-test; negative control vs. cold: paired t-test; and, cold vs. meal: paired t-test), or as otherwise stated. Correlations between variables were examined with Pearson's and Spearmen's rank correlation. P-value of less than 0.05 was considered as statistically significant. Data are presented as mean ± SEM, unless stated otherwise. N represents number of subjects, details of groups and statistical parameters can be found in the figure legends. Since no pervious data exist regarding BAT postprandial NEFA uptake, hence sample size power calculations were based on data from insulin stimulated glucose consumption in BAT, reported previously (Orava et al., 2011).

DATA AND SOFTWARE AVAILABILITY

The accession number for the RNA-Seq data presented in this article is GEO: GSE113764.

ADDITIONAL RESOURCES

Ethical review board of the Hospital District of Southwest Finland ethical review number ETMK: 45/180/2011.